Bioelectrochemistry 152 (2023) 108416

Contents lists available at ScienceDirect

Bioelectrochemistry

journal homepage: www.journals.elsevier.com/bioelectrochemistry

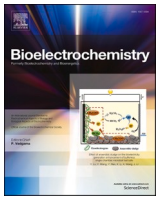

A disposable impedance-based sensor for in-line cell growth monitoring in CAR-T cell manufacturing

Zhaonan Liu [a,b], Xuzhou Jiang [a], Shuai Li [a], Jialei Chen [a,c], Chen Jiang [a,b], Kan Wang [a], Chuck Zhang [a,c,*], Ben Wang [a,b,c]

[a] Georgia Tech Manufacturing Institute, Georgia Institute of Technology, Atlanta 30332, United States
[b] School of Materials Science and Engineering, Georgia Institute of Technology, Atlanta 30332, United States
[c] H. Milton Stewart School of Industrial and Systems Engineering, Georgia Institute of Technology, Atlanta 30332, United States

ARTICLE INFO

Keywords:
Chimeric antigen receptor T cell
Impedance spectroscopy
Electrode polarization
Dielectric relaxation

ABSTRACT

This paper presents the development of low-cost, disposable impedance-based sensors for real-time, in-line monitoring of suspension cell culture. The sensors consist of electrical discharge machining (EDM) cut aluminum electrodes and polydimethylsiloxane (PDMS) spacers, both of which are low-cost materials that can be safely disposed of. Our research demonstrates the capability of these low-cost sensors for in-line, non-invasive monitoring of suspension cell growth in cell manufacturing. We use a hybrid equivalent circuit model to extract key features/parameters from intertwined impedance signals, which are then fed to a novel physics-inspired (gray-box) model designed for α-relaxation. This model determines viable cell count (VCC), a critical quality attribute (CQA) in cell manufacturing. Predicted VCC trends are then compared with image-based cell count data to verify their accuracy.

1. Introduction

Cell therapies have shown great potential and excellent clinical results in treating various cancers [1,2], blood disorders [3,4], and autoimmune diseases [5,6]. In recent years, U.S. Food and Drug Administration (FDA) has approved two types of chimeric antigen receptor (CAR)-T cell therapies [7,8], which is widely considered to be a milestone in cancer treatment. However, as autologous therapies, both approved CAR-T cell therapies are much more expensive than allogeneic cell therapies due to the non-reusability of the bioreactor or the parts that come into direct contact with cells. The extremely high costs hinder the accessibility of these promising treatments. Currently, one of the foremost demands in the CAR-T cell therapy industry is to bring the cost to a level affordable for average families and reimbursable to health insurance providers. Scaling up the cell manufacturing process and employing automated process control are two effective approaches to achieve this goal, as consumables and labor costs are the two major components in this industry. Both approaches require non-intrusive, in-line monitoring of critical quality attributes (CQAs).

Viable cell count (VCC) is a CQA that directly reflects overall cell growth and provides valuable information for decision-making in a cell manufacturing process. Mainstream methods for cell growth monitoring rely heavily on sampling and microscopy, which are usually labor-intensive and time-consuming. Although various technologies are now available to reduce the human labor involved in optical monitoring methods [9], most technologies are limited by the focus range and speed [10,11]. Therefore, these methods are always considered invasive and off-line during cell culturing.

Electric impedance spectroscopy is an alternative approach to achieving non-invasive and label-free cell growth monitoring by characterizing the change in electrical properties induced by cell expansion [11–14]. Probes embedded in the culturing system can monitor cell growth without sampling, thus avoiding disturbance and the chance of contamination in the culturing media. Aside from noninvasiveness, impedance measurements' primary merit is their selectivity in cell monitoring, as they only respond to viable cells. The selectivity grants impedance measurements the ability to monitor viable cell count, a CQA that is impractical to obtain by conventional optical methods without staining the cells. VCC can detect anomalies, provide harvest time instructions, and assess cell products to indicate overall growth. Besides VCC, this technique has also proven effective in monitoring cell viability, morphology, and orientation [15,16]. The past few decades

* Corresponding author.
E-mail address: chuck.zhang@gatech.edu (C. Zhang).

https://doi.org/10.1016/j.bioelechem.2023.108416
Received 22 November 2022; Received in revised form 17 March 2023; Accepted 18 March 2023
Available online 21 March 2023

have witnessed diverse impedance-based measurements for cell growth monitoring for a variety of purposes and applications, including electric cell-substrate impedance sensing (ECIS), electric impedance spectroscopy (EIS), impedance flow cytometry (IFC), and impedance sensing for cells cultured in 3D scaffolds.

Despite their great potential, impedance-based cell growth sensors face several hurdles in their application in in-line cell growth monitoring in cell manufacturing processes. A knowledge gap exists in describing the electrical property of a living cell and its dependency on different attributes of the cell. Researchers have studied the dependence on VCC [17], cell size [18], cell morphology [19], cell viability [20], and culture media conductivity [21]. However, a comprehensive analysis of the combined effect of these factors and an expedition toward distinguishing them is lacking. Multiple factors, including VCC, cell size, and culturing media conductivity, all contribute to the electrical property of the cell suspension, thus affecting impedance readings simultaneously [18]. In a cell manufacturing process, these factors are all constantly changing. On the one hand, the sensor readings contain all that information, paving the way to simultaneously sensing multiple CQAs. On the other hand, the intertwined information poses a significant challenge to analyzing the sensor readings. A possible approach to overcome this knowledge gap is to study the impedance spectrum in a wider frequency range. Two dielectric relaxation processes have been found to have a close relationship with particle size and concentration in a colloid suspension system: α-relaxation and β-relaxation. β-relaxation, appearing at the kHz-MHz frequency range, is well-explored in biomass characterization. However, α-relaxation (also known as low-frequency dielectric dispersion (LFDD), appearing around the kHz frequency range, is seldom studied. The mechanism of α-relaxation is not fully clear to date, but great potential and research opportunities lie in it. In this work, we have developed a novel physics-inspired method to analyze the α-relaxation signal with promising results in VCC monitoring.

The two aforementioned low-frequency dielectric relaxation processes inevitably run into the electrode polarization (EP) effect [22]. Most sensors rely on expensive materials and complex setups to eliminate or minimize the EP effect. Some researchers use platinum for electrodes, conduct surface treatment, or adopt complex experimental setups to eliminate or reduce the EP effect [23,24]. Since all approved CAR-T cell therapies available today are autologous, cells manufactured for each patient differ. Parts in the bioreactor that have direct contact with cells typically cannot be reused for another patient, including impedance-based cell growth sensors. Thus, a disposable impedance-based cell growth sensor is the right choice for CAR-T cell manufacturing. To reduce the cost, the materials used for the sensors must be low-cost and biocompatible.

This paper designs and fabricates disposable 3D sensors using low-cost materials and a compact design. The sensors adopt a two-electrode parallel-plate design consisting of electrical discharge machining (EDM) cut aluminum electrodes and polydimethylsiloxane (PDMS) spacers. The sensors can be easily customized for applications in different bioreactors to achieve low-cost, in-line, and non-invasive monitoring of the suspension cell growth in cell manufacturing. The parallel-plate sensor can provide reliable localized cell density information with a well-defined sensing region with an almost uniform electric field.

A novel physics-inspired method analyzes the impedance data collected with the measurement system. We first use a hybrid equivalent circuit model to extract features from the intertwined impedance signals. Then we plug selected features into a physics-inspired model to predict VCC. Finally, the trend of predicted VCC is compared with image-based cell count data to verify the accuracy and determine unknown coefficients in the model. Data collected from multiple cell expansion runs are used to validate our method. The results show that our approach is promising to monitor the suspension cell growth in cell manufacturing and offer critical information, such as abnormality and estimated harvesting time, for decision-making in practice.

2. Materials and experimental methods

2.1. Cell culture

Human leukemic T-cells (Jurkat E6-1; American Type Culture Collection, ATCC) were cultured in an ATCC-formulated culture medium (RPMI-1640; GE Healthcare) with 10% fetal bovine serum, 2 mM L-glutamine, 10 mM 4-(2-hydroxyethyl)-1-piperazineethanesulfonic acid (HEPES), 1 mM sodium pyruvate, 4500 mg/L glucose, and 1500 mg/L sodium bicarbonate in a 75 cm^2 Petri Dish (NuncEasYFlask; ThermoFisher Scientific). All of the cells were cultured in a humidified incubator controlled at 37 ℃ and 5% CO_2, and all the culture media were pre-heated to avoid the temperature effect on the impedance measurement. The cells were counted by an automated cell counter (TC20; Bio-Rad Laboratories, Inc.), and the concentration was maintained between 1×10^5 and 1×10^6 cells/mL.

2.2. Fabrication and assembly of the disposable 3D impedance sensor

The disposable impedance-based sensor consists of a pair of parallel-plate aluminum electrodes and PDMS (Sylgard 184, Dow Corning) spacers to maintain a gap between the two electrodes. Fig. 1(a) presents the process flow of the disposable impedance-based sensor. Firstly, a precise EDM cut a square bottom electrode with a thin tail from a 0.4 mm thick aluminum plate (Corrosion-Resistant 3003, McMaster-Carr®). The edge length of the electrode ranged from 9 mm to 16 mm. The surface of the cut aluminum plates was sanded using P600 sandpaper to remove any residual oil in the manufacturing process. The tail was gently bent up with an interconnection wire carefully soldered to its end with stable and low contact resistance. Secondly, four cured PDMS spacers were aligned to the four corners of the bottom electrode. The thickness of the spacer varied from 0.5 mm to 2 mm, while the edge length of the spacer was 2 mm. Then, the top electrode was aligned on the PDMS spacers to form the parallel plate structure. One uncured PDMS drop was placed at each corner and cured at 125 ℃ for 20 min to bond the electrodes and spacers. Fig. 1(b) shows a photo of an as-assembled sensor. A sensor array for distributive sensing in the bioreactor was completed by repeating the above procedures. The assembled sensors were immersed in ethanol for 10 min and completely air-dried under UV light for 2 h in a biological safety cabinet (BSC) to sterilize the entire structure. At last, a layer of uncured PDMS painted on the bottom of the sensors glues them to the Petri dish. The sensor array and Petri dish were placed inside the BSC for 48 h at room temperature to cure the PDMS layer completely.

2.3. Impedance measurement for the sensor array

Fig. 2(a) presents the schematic of the impedance measurement system, while Fig. 2(b) displays photographs of the actual apparatus. Impedance spectra were measured using an LCR meter (E4980AL; Keysight Technologies) with a sinusoidal signal of 22 mVrms, based on the literature [25]. The measurements were taken at 15 selected frequencies ranging from 300 Hz to 100 kHz, with the sensor array connected to the LCR meter sequentially through a multiplexer (PXI-2530B; National Instruments). To acquire impedance data of the sensor array, we utilized LabVIEW-coded customized software that recorded the data every 15 min. To balance the need for speed and accuracy in measurement, we opted for using 15 frequencies with 25 data points per frequency. This configuration provided sufficient information for capturing the most critical features in the impedance spectra, while also ensuring a short data acquisition time that is imperative for in-line cell monitoring. Before experimentation, all sensors were short-circuited by clipping their two electrodes together to account for any impedance introduced by the multichannel system, which was then subtracted from the measured results obtained during cell culture to minimize system error.

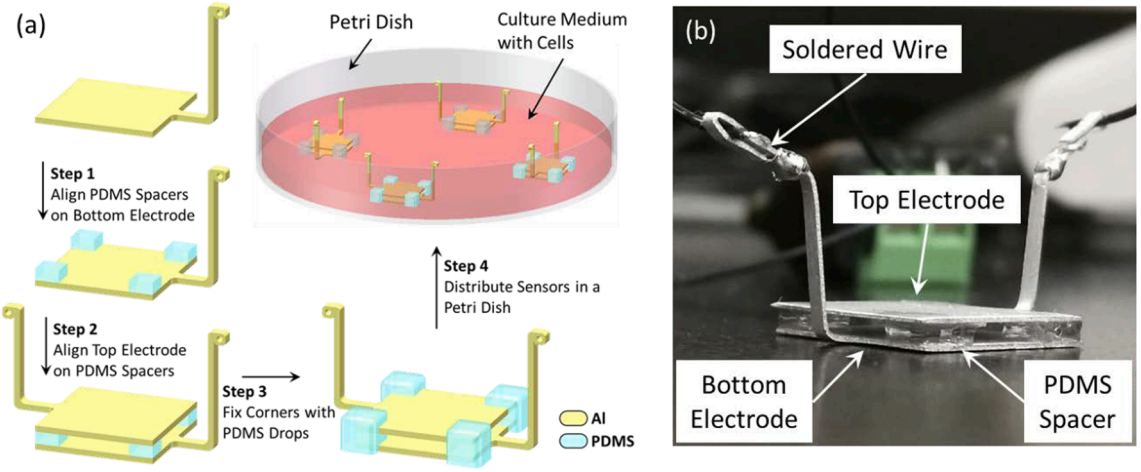

Fig. 1. (a) Process flow of an impedance-based biosensor; (b) Photo of an as-fabricated impedance-based biosensor.

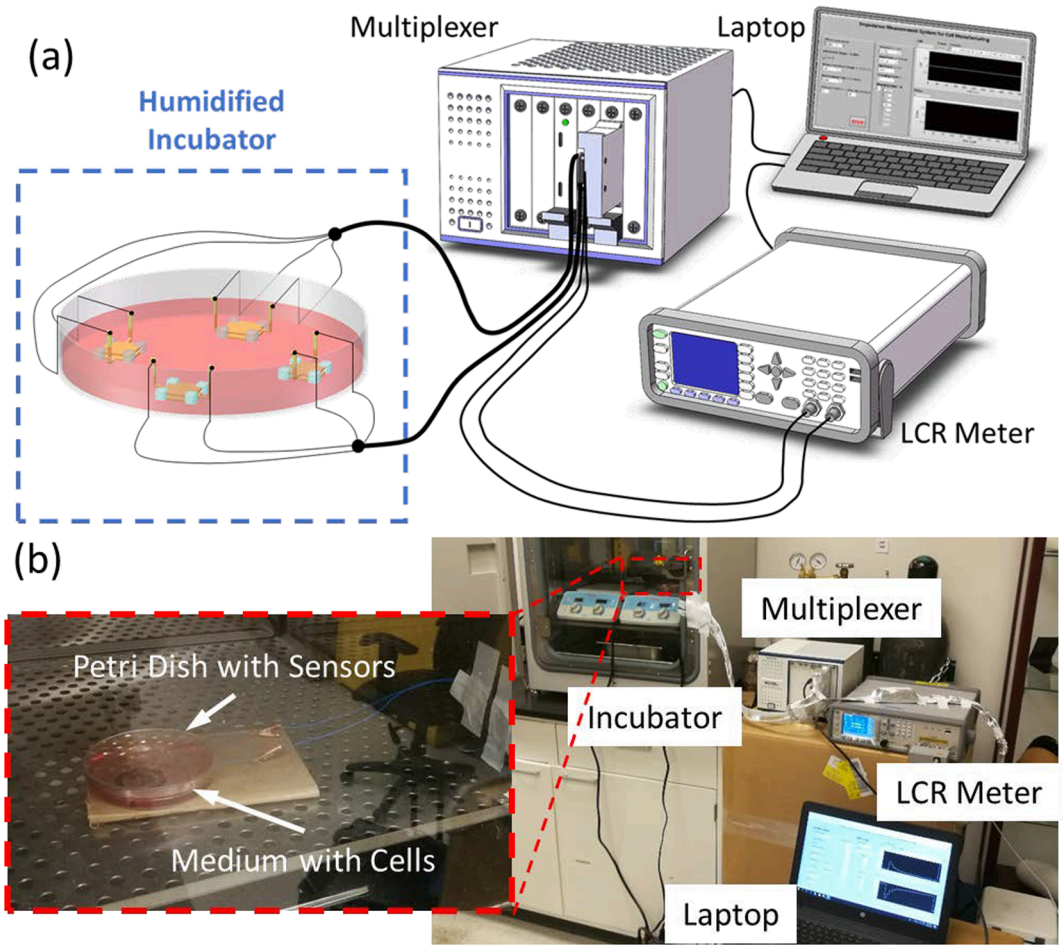

Fig. 2. (a) Schematic of the multiplexed impedance measurement system with a biosensor array; (b) Photos and details of the impedance measurement setup.

3. Data process methods

This section presents our new data process methods to understand the relationship between the measured impedance signal and VCC. As shown in Schematic 1, the collected data are processed in three steps. First, we preprocess the raw impedance data, removing or minimizing noise and system error. After data preprocessing, we define and extract features from impedance signals using a two-component equivalent circuit model. Then, we feed the extracted features into a physics-inspired model developed in this paper. Finally, we use the image-based cell count data to evaluate the model and determine the unknown coefficients.

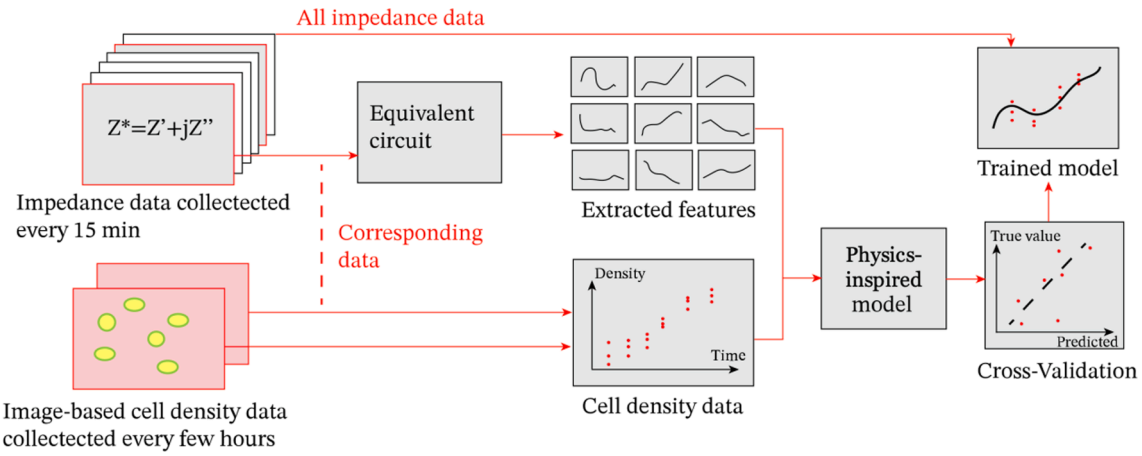

Schematic 1. Flowchart of the data processing methods. The plots in the image do not represent data in this paper.

3.1. Data preprocessing

3.1.1. Averaging and noise filtering

The LCR meter collects impedance data for 15 selected frequencies ranging from 300 Hz to 100 kHz. At each frequency, the instrument measures 25 impedance data points, and we average the 25 data points to obtain one impedance for the input of the spectrum fitting algorithm. Due to the high humidity in the incubator and the Petri Dish, the exposed metallic cables sometimes, cause erroneous data with very large variations. We also calculate the standard deviation from each set of raw impedance data and use it as a filter to remove data with large noise. If the ratio of the standard deviation to the mean value for any frequency exceeds 0.02, the entire spectrum over 15 frequencies is discarded for that measurement.

3.1.2. System error correction

As mentioned in Section 2.3, a short-circuit test is conducted before each experiment for system error correction. The short-circuit test data is collected and preprocessed in the same way as the experimental data described in Section 3.1.1. Then, we subtract the averaged short-circuit data from each averaged experiment data to obtain the corrected impedance spectra used for feature extraction in Section 3.2.

3.2. Equivalent circuit model for feature extraction

3.2.1. Two-component equivalent circuit model

Raw data collected from the LCR meter are impedance spectra containing information from the cell culture between the two electrodes. First, we need to extract features from the sensor readings to disentangle the signal from different sources and find the relationship between sensor readings and cell growth. In this research, we deliberately choose a compact design and low-cost materials to evaluate their potential in scaled-up applications. However, these sensors inevitably run into significant noise due to the EP effect. A two-component equivalent circuit model processes the raw impedance data from the LCR meter to account for the EP effect. The model consists of two components in series:

- Cell suspension component;
- EP effect component.

As shown in Schematic 2, the cell suspension component describes the electrical property of the cell suspension between the two electrodes, while the EP effect component describes the electrical property in the vicinity of the electrode surface. Since the current goes through the two components consecutively, they are supposed to be in series. We adopt the conductivity Debye relaxation model for the cell suspension component [21] and the constant phase element (CPE) model for the EP effect component [26].

The study of electrical properties of cell suspension has stemmed from the study of colloidal suspensions. When applied with an AC electric field, colloids suspended in liquid electrolytes exhibit Maxwell-Wagner (M-W) dielectric relaxation [27]. M-W relaxation process happens at the interface of two different materials. An ideal M-W relaxation is a single-time relaxation described with a Debye relaxation model:

$$\varepsilon^*_{\mathrm{D}}(\omega) = \frac{\Delta\varepsilon}{1 + j\omega\tau} + \varepsilon_{\mathrm{h}}, \tag{1}$$

where $\omega = 2\pi f$ is the radial frequency of the input AC signal, and the complex permittivity spectrum $\varepsilon^*_{\mathrm{D}}(\omega)$ is determined by the relaxation time constant τ, relaxation strength $\Delta\varepsilon$, and permittivity at the high-frequency limit ε_{h}. Considering the lossy nature of the cell culture in the culturing media, we adopt the conductivity Debye relaxation model:

$$\sigma^*_{\mathrm{D}}(\omega) = \frac{\Delta\sigma}{1 + j\omega\tau} + \sigma_0, \tag{2}$$

where the complex conductivity spectrum $\sigma^*_{\mathrm{D}}(\omega)$ is determined by the relaxation time constant τ, relaxation strength $\Delta\sigma$, and conductivity at the low-frequency limit σ_0. In most scenarios, relaxation processes observed in electrolytes are non-ideal, deviating from the Debye model.

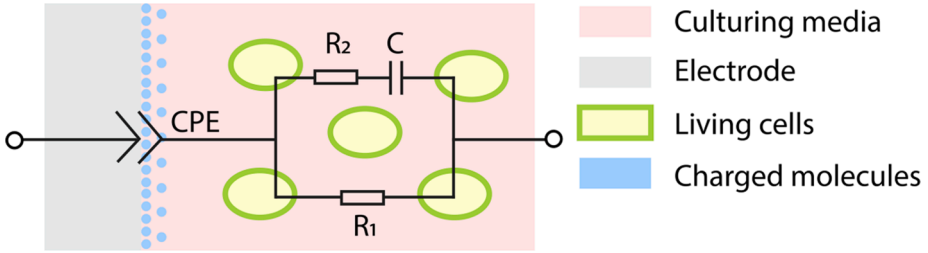

Schematic 2. The two-component equivalent circuit consisting of a cell suspension component and an EP component in series.

Colloidal suspension systems often adopt Cole-Cole relaxation to describe their dielectric behavior [28]. However, based on initial analysis of the experimental data, we have found that the conductivity Debye relaxation is enough for describing the experimental data. Moreover, since the Cole-Cole relaxation model is close to a CPE component in series or parallel to resistors, the feature extraction algorithm may wrongly attribute the features to an incorrect component. To better integrate with the EP effect component, the cell suspension component (conductivity Debye model) can be rewritten as an equivalent circuit model:

$$Z^*_{\text{Cell}} = \frac{1}{\frac{1}{R_2+\frac{1}{j\omega C}}+\frac{1}{R_1}}, \tag{3}$$

where $R_1 = \frac{1}{C_0\sigma_0}$, $R_2 = \frac{1}{C_0\Delta\sigma}$, $C = C_0\Delta\sigma\tau$. As shown in Schematic 2, in the equivalent circuit, capacitor C is in series with resistor R_2, and the subcircuit is in parallel with resistor R_1. C_0 is the cell constant accounting for the sensor geometry. Here, we can assume $C_0 = 1$ since it is a real constant, and we can let the actual information carried with $\Delta\sigma$ and σ_h. The effect of the cell constant C_0 can be neutralized with calibration.

It is worth pointing out that R_1, R_2 and C also have physical significance. The subcircuit of R_2 and C in series can be viewed as a dielectric Debye relaxation model with the permittivity at the high-frequency limit $\varepsilon_h = 0$, while R_1 indicates conductivity at the low-frequency limit. With $C_0 = 1$, C is equivalent to $\Delta\varepsilon$ in Debye dielectric relaxation model. The conductivity Debye model can be rewritten in a permittivity fashion:

$$\varepsilon^*_{\text{D}}(f) = \frac{\Delta\varepsilon}{1+j\omega\tau}+\frac{\sigma_0}{j\omega}, \tag{4}$$

where $\Delta\varepsilon = \frac{C}{C_0} = \Delta\sigma\tau$. Our initial analysis shows that the permittivity at the high-frequency limit ε_h is very close to 0, while the conductivity at the low-frequency limit σ_0 is not negligible.

Three or four dielectric relaxation processes are typically observable in cell suspensions: α, β, γ, and sometimes δ-relaxation, depending on the specific system under test [27]. The relaxation process most widely used to indicate VCC is the β-relaxation, which appears at kHz-MHz frequencies. This relaxation process is well-explored and has proven capable of indicating VCC. The α-relaxation, appearing at around kHz range, is much less explored in suspension systems, and its potency in indicating VCC is not verified. However, the α-relaxation has some advantages over the β-relaxation. Since the frequency range of the β-relaxation is higher, it is more prone to electromagnetic and stray capacitance noises. Coaxial cables are usually necessary to protect against those noises, making the sensor bulky and expensive. The α-relaxation with a lower frequency range is less reliant on noise-canceling techniques such as coaxial cables, allowing more flexibility in the sensor design. In this work, we have found that α-relaxation also has the capability to indicate cell density with parallel-plate sensors. Specifically, we use linear regression to find out the best combination of the extracted features and found that a certain combination of the relaxation strength $\Delta\varepsilon$ and the time constant τ of the α-relaxation can accurately indicate cell density.

EP effect has been bugging researchers from obtaining an accurate spectrum that reflects the dielectric properties of the object under test, especially in analyzing liquids. Ions within the liquid can be blocked by the electrodes, while they are also diffusing due to thermal fluctuations, resulting in an electric double layer that behaves like a non-ideal capacitor. Experimental and mathematical methods have been developed to eliminate or reduce the influence of the EP effect [24]. Experimental methods will likely raise the cost of the sensors since they require expensive metals or complex sensor design and measurement settings, which contradicts our goal of lowering the cost. Moreover, some mathematical approaches show promising results in compensating for the EP effect [22]. Therefore, we focus on mathematical methods to alleviate the EP effect. The EP effect can be modeled as a constant phase element (CPE) [29]:

$$Z^*_{\text{EP}} = \frac{1}{Q(j\omega)^n}, \tag{5}$$

where $Q > 0$ quantifies the strength of the EP effect, and $n \in [0, 1]$ is the phase of the CPE component. When $n = 1$, the CPE component describes purely capacitive behavior, while for $n = 0.5$, it describes purely diffusive behavior. The CPE model is appropriate in describing the EP effect on aluminum electrodes [30].

Since the EP effect occurs in the vicinity of the electrodes while most cell suspension is in between, the EP effect component and cell suspension component should be in series (See Schematic 2). Thus, the total impedance can be expressed as:

$$Z^*_{\text{total}} = Z^*_{\text{Cell}} + Z^*_{\text{EP}}, \tag{6}$$

where Z^*_{Cell} and Z^*_{EP} are as defined in Equation (2) and Equation (5). The final model includes five parameters: R_1, R_2, C, Q and n. From these five parameters we can derive physically significant features including $\Delta\sigma$, $\Delta\varepsilon$, τ, σ_0, and σ_h.

3.2.2. Loss function

Under sinusoidal AC conditions, complex permittivity and impedance spectra bear the same information but convey different messages, while both have physical significance. In other words, the complex electrical variable has two forms: permittivity and impedance. When this two-sided coin encounters a fitting problem, a dilemma arises: A fitted curve with minimum error in impedance may be non-optimal in permittivity and vice versa. This arose because the transformation between impedance and permittivity is not linear, and what was very close in numerical values to each other may become far away after the transition. In cases where impedance has more importance over permittivity, data are presented and fitted using impedance (e.g., transepithelial/transendothelial electrical resistance (TEER) [31]). In contrast, in other cases where permittivity is dominant, permittivity is used instead (e.g., dielectric properties of liquids [32]). However, impedance and permittivity are both essential and intertwined in this research. Previous research has addressed this property of impedance data with different weights according to the frequencies [33]. This technique balances the significance of high-frequency and low-frequency data while leaving flexibility to change the weights for the best result. However, using this technique usually results in a lack of reasoning for the choice of weights. To better address this unique property of impedance spectra, we deliberately define a distance function to balance impedance and permittivity. By taking the logarithm on permittivity and impedance, we find out that the distance is preserved in the transition:

$$\ln\varepsilon^*_1 - \ln\varepsilon^*_2 = \ln\frac{1}{jC_0\omega Z^*_1} - \ln\frac{1}{jC_0\omega Z^*_2} = \ln Z^*_2 - \ln Z^*_1 \tag{7}$$

Formatting data into $\ln Z^*$ (and thus defining the distance as $||\ln Z^*_1 - \ln Z^*_2||$) will result in a consistent definition of distance, whether impedance or permittivity is used. We estimate those eight parameters by minimizing the following loss function:

$$L(\widehat{\mathbf{Z}}^*, \mathbf{Z}^*) = \sum_{k=1}^{K} ||\ln\widehat{Z}^*_{f_k} - \ln Z^*_{f_k}||, \tag{8}$$

where $\widehat{Z}^*_{f_k}$ is the predicted impedance at the kth frequency in the frequency list using Equation (6), and $Z^*_{f_k}$ is the corresponding impedance measurements.

The eight parameters that reflex physics-based features are extracted from impedance data by minimizing the loss function defined in Equation (8). We employ the Basinhopping and Sequential Least Squares

Programming methods to solve the global minimization problem [34–36]. Due to the nonlinear and non-convex nature of the optimization problem, the feature extraction is non-trivial even with the complete equivalent circuit model and the fitting tool in hand. To avoid local optima, we initially try random initial values to find the best one for the first valid impedance spectrum. Then, we use the extracted features for the first valid spectrum as the initial guess of the second valid spectrum, and so on. This approach leverages the similarity between two adjacent spectra acquired within 15 min, making the previous fitted result a good guess for the upcoming spectrum, unless large external noise is introduced.

3.3. Physics-inspired model for VCC prediction

VCC is an essential CQA in cell manufacturing, guiding decision-making in cell culture processes. We use a physics-inspired (gray-box) model to predict VCC and evaluate its accuracy with image-based cell count data. Unlike a physics-based model, which solely relies on knowledge, and a data-driven model, which solely depends on data, a physics-inspired model involves both. A physics-inspired model takes advantage of knowledge summarizing past observations while bypassing the current knowledge gap to produce fruitful outcomes. Our physics-inspired model generalizes existing formulas and uses experimental data to determine uncertain parameters. In Section 3.2, five features are extracted from experimental data, and features with physical significance are reconstructed. Among those features, we have found two features that prove effective in predicting VCC with the physics-inspired model: $\Delta\varepsilon$ and τ. The physics-inspired model can be expressed as below:

$$\log \mathrm{VCC} = \log c_1 + c_2 \log \Delta\varepsilon + c_3 \log \tau \tag{9}$$

where $c_1 > 0$, c_2 and c_3 are parameters to be determined in the linear regression.

3.3.1. Maxwell-Wagner relaxation

We use a physics-inspired model to relate the extracted features with VCC. The model is inspired by a dielectric relaxation model where cells are assumed as colloidal suspensions where the colloids have thin, insulating shells (cell membranes) and conducting kernels (cytoplasm). Those simplified cells can induce Maxwell-Wagner relaxation. In the relaxation process, ions in the cytoplasm and the culture media move under AC electric field force and stop and gather when they reach the cell membrane. Since the cell membrane is only insulating if viable and becomes permeable if dead, only viable cells can be detected with the impedance sensor, and dead cells are transparent. This feature is a valuable addition to monitoring total cell count, as impedance sensors are now capable of exclusively monitoring viable cells.

Maxwell-Wagner relaxation gives rise to α-relaxation and β-relaxation in a spherical single-shelled cell model. The β-relaxation of spherical single-shelled cells can be described in the equation below [27]:

$$\Delta\varepsilon = \frac{9 r C_\mathrm{m}}{4\varepsilon_0} P, \tag{10}$$

where the relaxation strength $\Delta\varepsilon$ is proportional to cell radius r, cell volume fraction P, and specific capacitance of the cell membrane C_m. ε_0 is the vacuum dielectric constant. Since the relaxation strength $\Delta\varepsilon$ is proportional to cell volume fraction P, $\Delta\varepsilon$ is often used to indicate viable cell concentration. Noticing that viable P is equal to the product of VCC and cell volume, we can rewrite Equation (10) as:

$$\mathrm{VCC} = \frac{\Delta\varepsilon\varepsilon_0}{3 C_\mathrm{m} \pi r^4}, \tag{11}$$

$\Delta\varepsilon$ alone is sufficient to predict VCC, given that the average cell radius does not change much. However, in T-cell culturing, such assumptions do not hold. T-cells grow dramatically in size when activated and start to multiply. In our experiments, the cells are thawed and centrifuged together, and thus they may multiply synchronously to some extent, resulting in a variation in the average size as they expand [37]. Therefore, we have to include more features to predict cell radius r.

According to previous research [21], cell radius r can be reflected by the time constant τ of Maxwell-Wagner relaxation:

$$r = \frac{2\tau\kappa_\mathrm{i}\kappa_\mathrm{a}}{C_\mathrm{m}(\kappa_\mathrm{i} + 2\kappa_\mathrm{a})}, \tag{12}$$

where κ_i is the conductivity of cytoplasm, and κ_a is the conductivity of culture media. Assuming that κ_i, κ_a and C_m are constants, r is proportional to τ. Plugging this relationship into Equation (11), we have the following equation:

$$\mathrm{VCC} = c_1 \Delta\varepsilon \tau^{-4}, \tag{13}$$

where c_1 is a calibration coefficient. Since impedance measurements are sensitive to changes in electrode geometries, c_1 is expected to change between different experiments due to the inevitable error introduced in the sensor manufacturing process. Although Equations (10–13) are meant for β-relaxation rather than α-relaxation, we obtained insights into the possible relations between dielectric features and VCC: they may be governed by a power-law.

3.3.2. α-relaxation and physics-inspired model

As indicated previously, α-relaxation is a dielectric relaxation process typically appearing at around kHz frequencies. Although α-relaxation has large relaxation strength, potentially making it a good indicator of the electrical property of the system under test, researchers still seldom use it to indicate cell density in cell cultures or concentration in colloid suspensions for the following two reasons. First, the mechanism of α-relaxation is not fully explained today. Researchers have made a great effort to study this phenomenon in colloid suspension systems and made significant progress, but there are still discrepancies between the theoretical and experimental behaviors [38]. Second, the α-relaxation frequency range largely overlaps with the EP effect, making it challenging to observe. In our work, we try to extract highly accurate α-relaxation features and relate them to image-based cell density data with a physics-inspired model to overcome or bypass the above-mentioned difficulties.

Inspired by Equations (10–13), the extracted features of α-relaxation could also have a power-law relationship with cell density. Power law assumes that the relationship between the parameters holds for all scales, which is in principle not valid for cell suspension systems. However, the cell density of cell cultures is usually confined within a specific range since the cells may not grow well otherwise. The power law will likely be a good approximation in this confined range. Therefore, we develop a physics-inspired model from Equation (13) to incorporate a data-driven method with the physical knowledge. Namely, we assume a power law between all variables in Equation (13), where all the exponents are treated as unknown parameters to be trained by experimental data. The untrained physics-inspired model can be expressed as below:

$$\mathrm{VCC} = c_1 \Delta\varepsilon^{c_2} \tau^{c_3}, \tag{14}$$

where c_1, c_2, and c_3 are calibration coefficients. Taking logarithms on both sides, we have:

$$\log \mathrm{VCC} = \log c_1 + c_2 \log \Delta\varepsilon + c_3 \log\, \tau, \tag{15}$$

the base of the logarithm can be chosen for arithmetic or algorithmic convenience. In this form, the training problem reduces to linear regression.

4. Results and discussion

4.1. Feature extraction

The impedance spectrum is automatically acquired with the LCR meter every 15 min. However, image-based cell count data used to train the model are much less frequently obtained since the process involves manual sampling and the consumption of lab supplies. Therefore, only a few impedance spectra with corresponding image-based cell count data are necessary for model training.

Selected data are fitted with Equation (6) as the model and Equation (8) as the loss function. Fitted results are visualized in both frequency-implicit and frequency-explicit plots in Fig. 3. Each spectrum has a minimal fitting error (RMSE $< 2\Omega$), indicating that the fitted model has captured the most significant features in the spectra acquired. The extracted and reconstructed features are shown in Fig. 4.

The extracted and reconstructed features show some patterns that may provide some insights into what happened in the culturing process. All features experience a steep change within the first few hours, which may reflect the cell culture and sensor system's stabilization. The cell suspension may undergo a dramatic temperature change since the culture media is refrigerated until use. Also, the microscopic roughness on the surface of aluminum electrodes may result in a wet-in process, which could significantly impact the acquired impedance. After 35 h, Q and n experience a steep change, indicating a disruption in the electrode surface, most likely due to the growth of microorganisms such as yeast and bacteria, which stick to surfaces. The cell culture also turns turbid at the end of the experiment, likely indicating bacteria or yeast contamination. Due to the disruption of the electrode surface, the impedance data collected after 35 h since the start may not reflect cell density effectively. On the bright side, this could indicate contaminant microorganism growth and inform the researchers and manufacturers in time to minimize the loss in time and consumables. Some features show spikes, oscillations, and plateaus, which are unlikely to reflect true cell density. These may have resulted from sources other than the change in cell density. The spikes and oscillations may have resulted from a loose connection in the sensing system, disruption in temperature due to sampling at room temperature, and local minima in the optimization process. The plateaus are the result of intentional algorithm design. As described in Section 3.1.1, the preprocessing algorithm filters out spurious data with large variances. In cases where the data is filtered out, the fitting algorithm repeats the previous data since it receives no new data. This helps preserve the previous fitting result for the initial guesses in the next impedance spectrum.

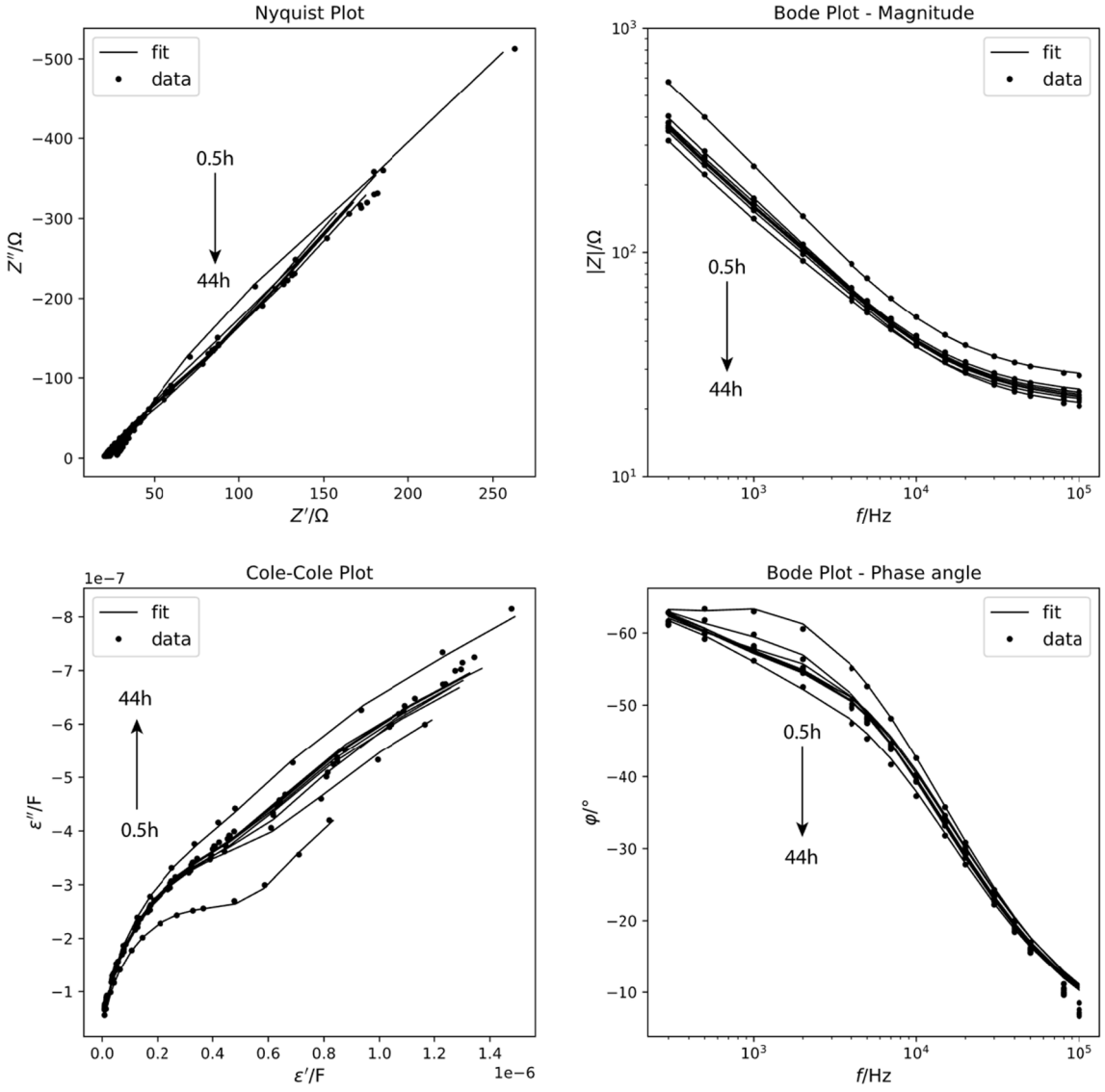

Fig. 3. Fitting results using the two-component equivalent circuit model. Fitting error is minimal with RMSE $< 2\ \Omega$ for all spectra fitting.

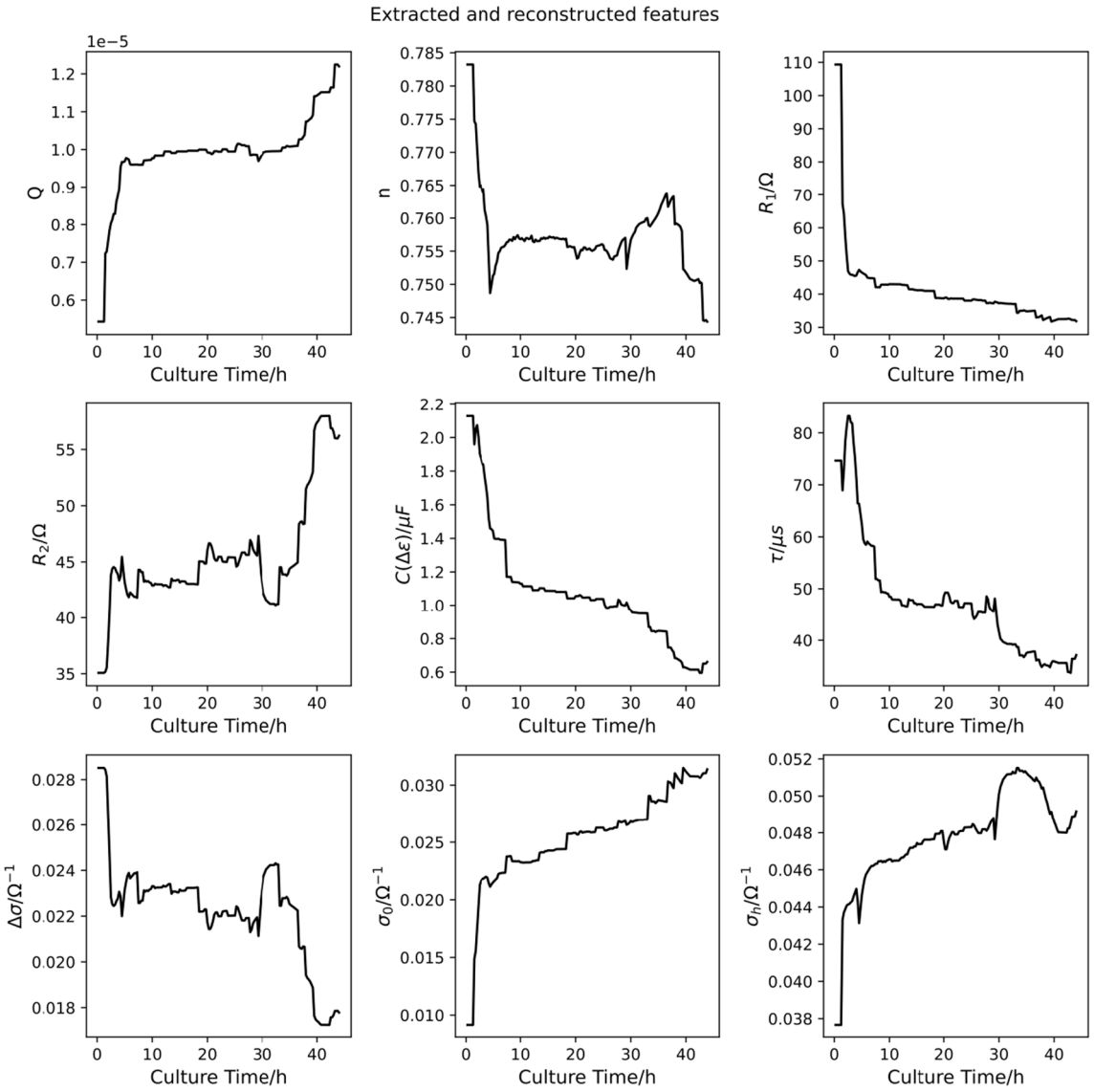

Fig. 4. Extracted and reconstructed features throughout the cell culturing process.

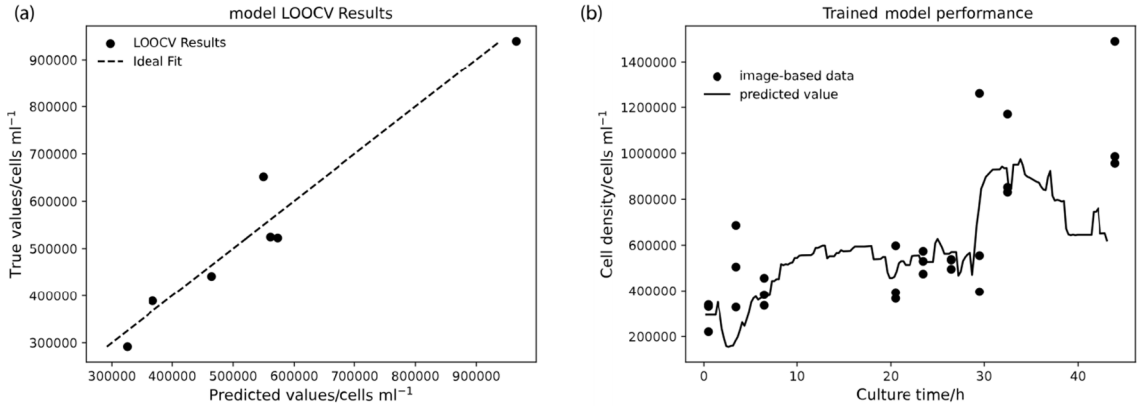

Fig. 5. (a) Results of LOOCV for all methods. The predicted value is plotted against the true value (averaged image-based cell density) for each data point. The straight line is where the predicted value equals the true value. Data points closer to the line are better predicted. Testing $R^2 = 0.937$. (b) Training result for VCC prediction using model trained with image-based cell count. Raw image-based cell density data are shown to show variability in cell counting. Training $R^2 = 0.964$.

4.2. VCC prediction

A physics-inspired model is developed in Section 3.3. We collected nine data points from the image-based cell counter throughout the cell culture process to train the physics-inspired model, where each data point is derived by averaging cell density from 3 samples independently collected from the cell culture. Initial analysis shows that the second and the ninth data points behave differently than the others, so these two data points are discarded for model training.

Leave-one-out cross-validation (LOOCV) is employed to distinguish effective training from pure hindsight. Among all seven data points, each one is selected in turn to be the testing data, and the rest are training data. LOOCV is used only for the evaluation of the methods. Training and testing errors are reported for each method. Since all parameters are taken logarithms before running the linear regression algorithm, the conversion back is necessary before evaluating the results. Final model is trained using all seven data points for optimum performance. The physics-inspired model achieves a testing R^2 of 0.937 in LOOCV, and a training R^2 of 0.964 for the trained model. Cross-validations and cell density predictions are plotted in Fig. 5. The trained physics-inspired model can be expressed as:

$$\mathrm{VCC} = c_1 \Delta\varepsilon^{1.70} \tau^{-3.91}, \tag{14}$$

where the calibration coefficient $c_1 = 0.0922$. c_1 may differ for each experiment, as the hand-made sensors inevitably introduce variability in the cell constant C_0. It is worth noting that this formula is not very far-away from Equation (13), which means that the formula for β-relaxation may also apply to α-relaxation with plausible results. The trained parameters may provide insights into the investigation of α-relaxation of living cells.

The untrained physics-inspired model has several adjustable parameters that can transform the extracted features into various possible curves. The linear regression algorithm can find the curve closest to the true values using all features. However, too much flexibility can lead to overfitting, where the model can only fit the training dataset but performs poorly in predicting new data. To avoid overfitting, we used LOOCV to evaluate the trained model's performance on new data. The physics-inspired model shows excellent results in LOOCV, indicating that the trained model revealed some nature about the cell suspension rather than fitting meaningless curves close to the data points by coincidence. We have also tried different combinations of extracted features to improve the physics-inspired model's accuracy, but most only show high accuracy in the training process but very low accuracy in LOOCV.

The trained physics-inspired model is applied to data collected from other cell culturing processes, and the predicted values are compared with the true values in Fig. 6. These results demonstrate that the power-law relationships suggested by the trained physics-inspired model is effective in reflecting cell density with moderate deviation. In fact, cell culturing in a Petri Dish without agitation may lead to variability in cell density at different locations in the cell suspension. The variation between the image-based cell density data collected clearly shows this effect. Taking this effect into account, the predicted cell density showing a moderate deviation from the image-based data is reasonable.

Since the scaling factor c_1 is different for each culturing process, it may contain case-specific parameters affecting sensor readings. For example, a small change in the distance between the two electrodes in our experimental setup may result in a significant difference in impedance readings. One possible approach to obtaining the case-specific parameters is to perform calibration before use. However, since the sensor is designed for single use, the calibration cost is relatively high. Another possible way to find these case-specific parameters and cancel

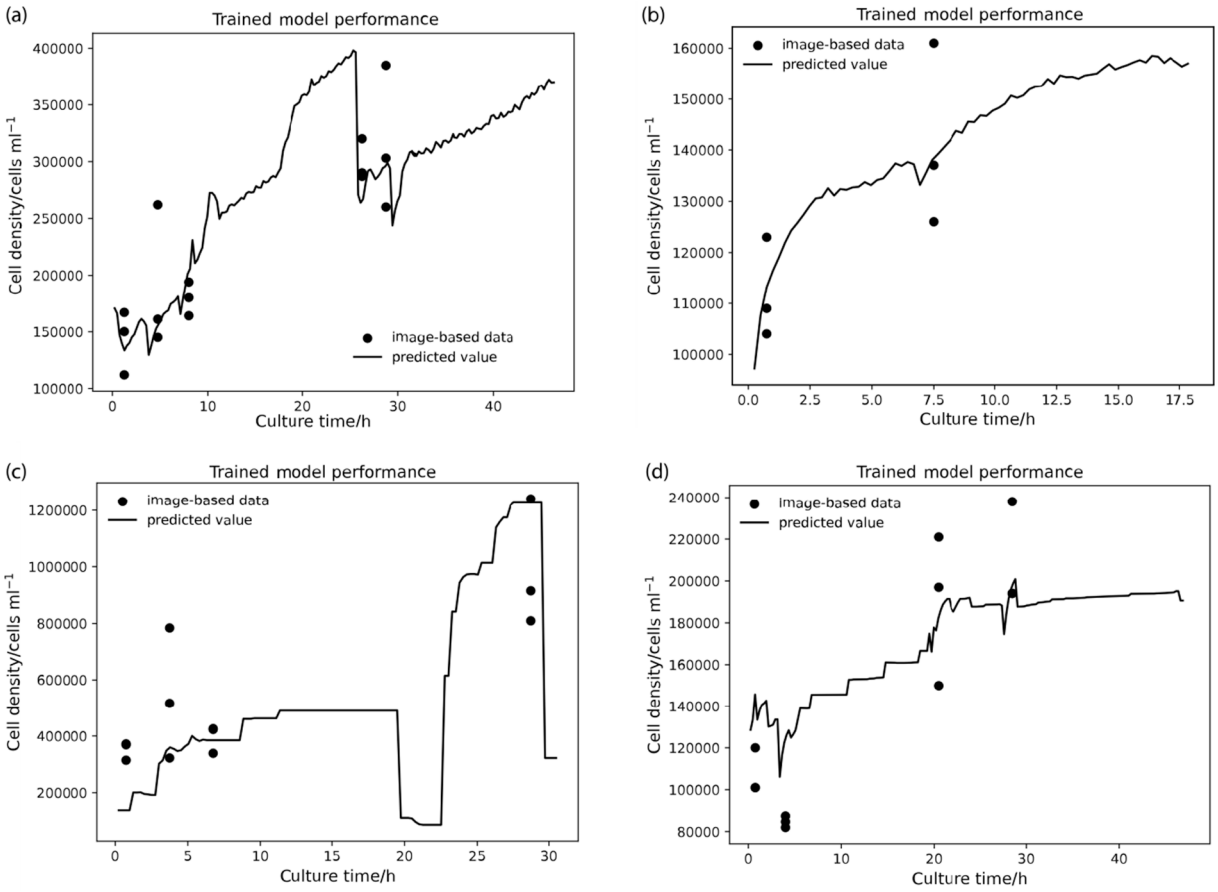

Fig. 6. Results of applying trained model to new data. All curves are rescaled by adjusting the value of c_1, while c_2 and c_3 are kept the same.

out their impact is to use multiple sensors with different geometries and apply a calibration-free framework to the sensing system [39].

The electric property of suspension of monodisperse, spherical cells is influenced by at least four independent variables: VCC, cell size, cell membrane capacitance C_m, and culturing media conductivity κ. In other words, this system has at least four degrees of freedom. However, in the physics-inspired method, we describe this system using only two variables: $\Delta\varepsilon$ and τ. The final model expressed in Equation (9) cannot fully describe the electric property of the cell suspension due to the lack of freedom, but the performance shown in the physics-inspired model suggests that those four variables mentioned above actually have some dependence on each other. For example, cell size may be relevant to C_m, since the cell membrane may behave differently in different stages within a cell cycle. Also, C_m may be relevant to κ, since they both are influenced by ion concentration and ion mobility. In scenarios where those dependencies change or disappear (e.g., different patients or different cell types), extra parameters and further analysis will be necessary.

The use of a power-law relationship in the physics-inspired method assumes that the relationship between variables is scale-invariant, which may not be valid in all cases. However, this assumption is a convenient and flexible mathematical model for data-driven analysis. Additionally, power-law is likely to be appropriate in cases where the variables, such as VCC and cell radius, do not change significantly over orders of magnitude during the cell culture process. If the cell culture process involves significant changes in the cell expansion over several orders of magnitude, further investigations may be necessary to determine the appropriate mathematical models.

5. Conclusion

In this research, we have designed and fabricated low-cost, disposable sensors for in-line monitoring of suspension cell growth and demonstrated their use in predicting cell density with a novel physics-inspired data analysis method. Consisting of EDM-cut aluminum parallel plates and PDMS spacers, the sensors show good biocompatibility and chemical stability. Raw impedance data is collected with our measurement system and then analyzed with a two-component equivalent circuit model to extract features. The feature extraction results show that the equivalent circuit model can nicely represent the cell suspension system under test. The extracted features are then plugged into our novel physics-inspired data analysis methods to predict viable cell count. Trained by image-based cell density values, the physics-inspired model shows excellent LOOCV performance with testing $R^2 = 0.937$. The trained physics-inspired model also shows good performance in predicting cell density in new data. With the physics-inspired data analysis method, the low-cost, disposable sensor can help decision-making, such as deciding on harvesting time and detecting abnormalities in cell manufacturing. The trained parameters in the physics-inspired model may also provide insights into research in low-frequency electrical properties of living cells.

Declaration of Competing Interest

The authors declare the following financial interests/personal relationships which may be considered as potential competing interests: Chuck Zhang reports financial support was provided by US Food and Drug Administration. Chuck Zhang reports financial support was provided by National Science Foundation. Chuck Zhang has patent METHODS OF DETERMINING VIABLE CELL COUNT AND IMPEDANCE-BASED BIOSENSORS FOR THE SAME pending to GEORGIA TECH RESEARCH CORPORATION.

Data availability

Data will be made available on request.

References

[1] C.H. June, et al., CAR T cell immunotherapy for human cancer, Science 359 (6382) (2018) 1361–1365.
[2] S.A. Rosenberg, N.P. Restifo, Adoptive cell transfer as personalized immunotherapy for human cancer, Science 348 (6230) (2015) 62–68.
[3] J.-A. Ribeil, et al., Gene therapy in a patient with sickle cell disease, N. Engl. J. Med. 376 (9) (2017) 848–855.
[4] A.A. Thompson, et al., Gene therapy in patients with transfusion-dependent β-thalassemia, N. Engl. J. Med. 378 (16) (2018) 1479–1493.
[5] C.T. Ellebrecht, et al., Reengineering chimeric antigen receptor T cells for targeted therapy of autoimmune disease, Science 353 (6295) (2016) 179–184.
[6] M. Miyara, Y. Ito, S. Sakaguchi, TREG-cell therapies for autoimmune rheumatic diseases, Nat. Rev. Rheumatol. 10 (9) (2014) 543–551.
[7] V. Prasad, Tisagenlecleucel—the first approved CAR-T-cell therapy: implications for payers and policy makers, Nat. Rev. Clin. Oncol. 15 (1) (2018) 11–12.
[8] P. Yin, keys to scale-up CAR T-cell therapy manufacturing, BioProcess Online (2017).
[9] S. He, et al., Automatic microscopic cell counting by use of deeply-supervised density regression model, in Medical Imaging 2019, Digital Pathology, 201SPIE.
[10] S.-M. Lee, et al., Real-time monitoring of 3D cell culture using a 3D capacitance biosensor, Biosens. Bioelectron. 77 (2016) 56–61.
[11] Y. Pan, et al., 3D cell-based biosensor for cell viability and drug assessment by 3D electric cell/matrigel-substrate impedance sensing, Biosens. Bioelectron. 130 (2019) 344–351.
[12] P. Ducommun, et al., On-line determination of animal cell concentration in two industrial high-density culture processes by dielectric spectroscopy, Biotechnol. Bioeng. 77 (3) (2002) 316–323.
[13] H. Fricke, Relation of the permittivity of biological cell suspensions to fractional cell volume, Nature 172 (4381) (1953) 731–732.
[14] R.A. Gerhardt, What is Impedance and Dielectric Spectroscopy? IEEE Instrum. Meas. Mag. 25 (4) (2022) 14–20.
[15] R. Zhang, et al., A cell viability assessment method based on area-normalized impedance spectrum (ANIS), Biosens. Bioelectron. 110 (2018) 193–200.
[16] P. Taraconat, et al., Detecting cells rotations for increasing the robustness of cell sizing by impedance measurements, with or without machine learning, Cytometry A 99 (10) (2021) 977–986.
[17] S. Metze, et al., Monitoring online biomass with a capacitance sensor during scale-up of industrially relevant CHO cell culture fed-batch processes in single-use bioreactors, Bioprocess Biosyst. Eng. 43 (2) (2020) 193–205.
[18] J.P. Carvell, J.E. Dowd, On-line measurements and control of viable cell density in cell culture manufacturing processes using radio-frequency impedance, Cytotechnology 50 (1) (2006) 35–48.
[19] M. Shaker, et al., An impedance-based flow microcytometer for single cell morphology discrimination, Lab Chip 14 (14) (2014) 2548–2555.
[20] N. Ke, et al., The xCELLigence system for real-time and label-free monitoring of cell viability, in: Mammalian cell viability, Springer, 2011, pp. 33–43.
[21] K. Asami, Low-frequency dielectric dispersion of bacterial cell suspensions, Colloids Surf. B Biointerfaces 119 (2014) 1–5.
[22] C. Chassagne, et al., Compensating for electrode polarization in dielectric spectroscopy studies of colloidal suspensions: theoretical assessment of existing methods, Front. Chem. 4 (2016) 30.
[23] H. Fricke, H.J. Curtis, The dielectric properties of water–dielectric interphases, J. Phys. Chem. 41 (5) (1937) 729–745.
[24] H. Schwan, Linear and nonlinear electrode polarization and biological materials, Ann. Biomed. Eng. 20 (3) (1992) 269–288.
[25] K. Su, et al., Integrated multifunctional cell-based biosensor system for monitoring extracellular acidification and cellular growth, Sens. Actuators, A 220 (2014) 144–152.
[26] Z. Kerner, T. Pajkossy, On the origin of capacitance dispersion of rough electrodes, Electrochim. Acta 46 (2–3) (2000) 207–211.
[27] H.P. Schwan, Electrical properties of tissue and cell suspensions, in: Advances in biological and medical physics, Elsevier, 1957, pp. 147–209.
[28] K.S. Cole, R.H. Cole, Dispersion and absorption in dielectrics I. Alternating current characteristics, J. Chem. Phys. 9 (4) (1941) 341–351.
[29] S. Emmert, et al., Electrode polarization effects in broadband dielectric spectroscopy, The European Physical Journal B 83 (2) (2011) 157–165.
[30] R. Cousseau, et al., Improved electrical model of aluminum electrolytic capacitor with anomalous diffusion for health monitoring, Math. Comput. Simul 131 (2017) 268–282.
[31] B. Srinivasan, et al., TEER measurement techniques for in vitro barrier model systems, SLAS Technology 20 (2) (2015) 107–126.
[32] J. Kindt, C. Schmuttenmaer, Far-infrared dielectric properties of polar liquids probed by femtosecond terahertz pulse spectroscopy, J. Phys. Chem. 100 (24) (1996) 10373–10379.
[33] M.D. Murbach, et al., impedance. py: A Python package for electrochemical impedance analysis, J. Open Source Software 5 (52) (2020) 2349.
[34] B. Olson, et al., Basin Hopping as a General and Versatile Optimization Framework for the Characterization of Biological Macromolecules, Adv. Artif. Intell. 2012 (2012), 674832.
[35] K. Levenberg, A method for the solution of certain non-linear problems in least squares, Q. Appl. Math. 2 (2) (1944) 164–168.
[36] J. Nocedal, S.J. Wright, Quadratic programming, Numerical Optimization (2006) 448–492.

[37] G. Banfalvi, Cell cycle synchronization of animal cells and nuclei by centrifugal elutriation, Nat. Protoc. 3 (4) (2008) 663–673.
[38] C. Grosse, A.V. Delgado, Dielectric dispersion in aqueous colloidal systems, Curr. Opin. Colloid Interface Sci. 15 (3) (2010) 145–159.
[39] J. Chen, et al., A calibration-free method for biosensing in cell manufacturing, IISE Transactions 54 (1) (2021) 29–39.